HHS Public Access

Author manuscript

Nat Biomed Eng. Author manuscript; available in PMC 2019 December 17.

Published in final edited form as:

Nat Biomed Eng. 2019 October ; 3(10): 783–795. doi:10.1038/s41551-019-0411-6.

Traceless aptamer-mediated isolation of CD8+ T cells for CAR-T cell therapy

Nataly Kacherovsky[1,4], **Ian I. Cardle**[1,2,4], **Emmeline L. Cheng**[1], **Jonathan L. Yu**[1], **Michael L. Baldwin**[2], **Stephen J. Salipante**[3], **Michael C. Jensen**[1,2,*], **Suzie H. Pun**[1,*]

[1]Department of Bioengineering, University of Washington, Seattle, WA, USA.

[2]Ben Towne Center for Childhood Cancer Research, Seattle Children's Research Institute, Seattle, WA, USA.

[3]Department of Laboratory Medicine, University of Washington, Seattle, WA, USA.

[4]These authors contributed equally: Nataly Kacherovsky and Ian I. Cardle.

Abstract

Chimeric antigen receptor (CAR) T-cell therapies using defined product compositions require high-purity T-cell isolation systems that, unlike immunomagnetic positive enrichment, are inexpensive and leave no trace on the final cell product. Here, we show that DNA aptamers, generated with a modified cell-SELEX (systematic evolution of ligands by exponential enrichment) procedure to display low nanomolar affinity for the T-cell marker CD8, enable the traceless isolation of pure $CD8^+$ T cells at low cost and high yield. Captured $CD8^+$ T cells are released label-free by complementary oligonucleotides that undergo toehold-mediated strand displacement with the aptamer. We also show that CAR-T cells manufactured from these cells are comparable to antibody-isolated CAR-T cells in proliferation, phenotype, effector function and antitumor activity in a mouse model of B-cell lymphoma. By employing multiple aptamers and the corresponding complementary oligonucleotides, aptamer-mediated cell selection could enable the fully synthetic, sequential and traceless isolation of desired lymphocyte subsets from a single system.

* spun@uw.edu and michael.jensen@seattlechildrens.org.

AUTHOR CONTRIBUTIONS

S.H.P. and M.C.J. conceived the idea and provided experimental advice and funding support. N.K. designed the project. N.K. and I.I.C. conceived, performed, and interpreted the experiments. N.K. designed and performed the SELEX procedure. I.I.C. and E.C. evaluated binding of aptamer libraries and select aptamers, and I.I.C., E.C., S.J.S., and N.K. analyzed NGS sequencing data. I.I.C. performed murine splenocyte and rhesus binding experiments. N.K., J.L.Y., I.I.C. and E.C. conducted receptor binding studies by siRNA knockdown and gene transfection. I.I.C. and N.K. conducted antibody competition and Octet studies. J.L.Y. and E.C. performed binding curve studies, and E.C. and I.I.C. evaluated aptamer binding to human PBMCs. N.K., I.I.C. and J.L.Y. optimized reversal agent and traceless cell isolation conditions. I.I.C. performed CAR T cell production and characterization studies. M.L.B. conducted *in vivo* tumor studies and bioluminescence imaging. I.I.C. prepared figures and performed statistical analyses. I.I.C., N.K., E.C., and S.H.P. wrote the manuscript.

COMPETING INTERESTS

S.H.P., M.C.J., N.K., and I.I.C. are co-inventors on two provisional patent applications (no. 62/699,438 and no. 62/779,946) on the aptamers and complementary reversal agents for traceless isolation described in this manuscript.

The clinical impact of T cell therapies is being rapidly realized with two recent FDA approvals for chimeric antigen receptor (CAR) T cell therapies treating acute lymphoblastic leukemia (ALL) and diffuse large B-cell lymphoma (Novartis's Kymriah and Gilead-Kite's Yescarta, respectively), as well as many promising results in clinical trials.[1–4] In addition to cancer, CAR T cells have also been generated as potential anti-HIV therapies.[5, 6] Currently, the generation and administration of autologous CAR T cell therapy involves harvesting and genetically manipulating T cells before reintroducing the engineered cells back to patients. The first step in the process, cell harvesting, requires high purity isolation of desired cell populations. For example, CAR T cells with defined 1:1 $CD4^+$ to $CD8^+$ cell populations have been reported to be more potent than either pure ($CD4^+$ or $CD8^+$ only) and unselected populations in animal models of leukemia and are also very effective in human clinical trials for ALL.[7, 8]

T cells for CAR T cell manufacturing are typically isolated from peripheral blood mononuclear cells (PBMCs) collected by leukapheresis. One method reported for use in clinical-scale T cell isolation is to sequentially isolate $CD8^+$ and $CD4^+$ T cells from the apheresis product by immunomagnetic positive enrichment (e.g. CliniMACS).[9] This approach can benefit from high purity and yield but may suffer from (i) high costs associated with biologically-produced antibodies, (ii) potential safety concerns stemming from a final cell population that may be still associated with antibody-coated magnetic beads, and (iii) low-throughput due to requiring multiple selection apparatuses in sequence.[10] Furthermore, the magnetic beads retained on the cells may prevent downstream selection of cell subsets that can be beneficial for therapy. While clinical selection strategies that immunodeplete undesired cell populations allow for untouched cell isolation and downstream positive selection of specific cell subsets, they also (i) introduce more costs by relying on a large panel of antibodies for depletion, (ii) reduce the yield by half as the apheresis product has to be split to obtain separate subsets of both $CD4^+$ and $CD8^+$ T cells, and (iii) can have low purity of target cells.[11, 12]

Streptamer-based cell selection technology has been reported that avoids some of these undesirable outcomes through fragment antigen-binding (Fab) constructs fused with a peptide tag that bind reversibly to magnetic beads coated with engineered streptavidin.[13–15] The Fabs can be released from the beads by competition with high-affinity D-biotin, and therefore must be engineered with relatively low receptor binding affinity so that they dissociate rapidly from the cell once released in the monovalent form.[14–17] While the extent of Fab internalization into the cells is unclear after release from the solid support, Fabs engineered with relatively low receptor binding are not significantly retained on the cell surface.[16] However, this method is still costly due to relying on biologically-produced engineered streptavidin and modified Fabs. Additionally, all the aforementioned approaches have low throughput and high supply requirements for $CD4^+$ and $CD8^+$ T cell isolation, relying on multiple selection apparatuses either in sequence or in parallel. Thus, despite technological advances in cell selection, an approach that comprehensively has low cost, traceless selection, and high throughput while maintaining reasonable yield and purity has remained elusive (Supplementary Table 1).

Nucleic acid aptamers, single-stranded oligonucleotides capable of binding target molecules, are an attractive alternative to antibodies and Fabs for cell selection. First developed in the 1990s,[18–20] aptamers can possess binding affinities comparable to or even higher than antibodies. Importantly, aptamers are produced synthetically as well-defined, low variability products with long storage stability, making them inexpensive and easy to manufacture.[21–23] Aptamers are commonly discovered through a library selection method known as SELEX (systematic evolution of ligands by exponential enrichment) and can be further optimized for chemical stability. With their favorable attributes, as summarized in Supplementary Table 1, the application field for aptamers has escalated in the last quarter century to encompass areas including sensing, purification, diagnostics, drug delivery and therapeutics.[24]

Here, we report a reversible aptamer selection technology for isolation of label-free $CD8^+$ T cells. Three main facets of the work are presented. First, we identified several high-affinity DNA aptamers specific for CD8 using a modified cell-SELEX procedure and validated binding characteristics of selected aptamers. We compared magnetic-activated cell sorting (MACS) with one of the aptamers to the antibody-based CD8 Microbead system that is used clinically and found that the aptamer isolates $CD8^+$ T cells from PBMCs with efficiencies comparable to the standard method. Second, we developed a method to reverse aptamer binding using a complementary oligonucleotide reversal agent to disrupt aptamer folding and show that $CD8^+$ cells can be released from aptamer-immobilized supports with high yield and purity using this approach. Finally, we generated and fully characterized CAR T cells from both our reversible aptamer selection approach and standard, antibody-based selection. CAR T cells isolated using traceless aptamer selection were phenotypically similar to those isolated using antibodies and exhibited nearly identical effector functions, both *in vitro* and *in vivo*. This aptamer-based selection approach therefore enables high efficiency, label-free, and inexpensive selection of T cells for potential clinical-scale cell therapy applications. With future discovery of other T cell-specific aptamers, such as a CD4 aptamer, this technique could be readily expanded for high-throughput, serial selection of multiple T cell populations from a single apparatus using a panel of aptamers and corresponding reversal agents.

RESULTS

Identification of T cell-binding aptamers by cell SELEX incorporating competitive and counter selection.

The generation of highly specific aptamers is critical for cell isolation applications. As our initial efforts to identify T cell-specific aptamers using either traditional protein-SELEX with recombinant proteins or cell-SELEX[25, 26] with engineered cell lines were unsuccessful and yielded aptamers with poor specificity, we hypothesized that both native display of receptors on cell surfaces afforded by cell-SELEX and increased stringency of selection provided by competitive selection[27] would be required to discover a T cell-specific aptamer. We therefore modified the published cell-SELEX protocol[28] to include both competitive selection (selection in the presence of relevant undesired cells) and counter selection (depletion of aptamers binding undesired targets) (Fig. 1). After a first round of positive selection against T cells using a single-stranded DNA library with 52 base pair random

region (10^{16} variants), the selected aptamer pool underwent multiple rounds of competitive/counter selection. Each round included competitive selection of T cell binding aptamers by incubation of aptamer pools with PBMCs followed by untouched T cell isolation and extraction of bound aptamers. Collected aptamers were then subjected to counter selection by incubation with J.RT3-T3.5, a $CD3^{-}CD4^{lo}CD8^{-}$ human T cell leukemia line, to remove aptamers binding non-selective surface proteins expressed on T cells. Selection stringency in each of five selection rounds was increased as summarized in Supplementary Table 2 and selection progress was monitored by flow cytometry (Supplementary Fig. 1). Binding to a subset of T cells was observed by round 3 and increased through round 5. Selection was halted after five rounds due to nonspecific binding to counter selection cells observed in round 5.

Aptamer pools from each round of selection were identified by next generation sequencing (NGS) using primers detailed in Supplementary Table 3 and analyzed using FASTAptamer[29]. Phylogenetic trees of the top 100 aptamers were generated using Figtree software (http://tree.bio.ed.ac.uk/software/figtree/)[30] and consensus motifs identified using MEME analysis[31] (Supplementary Fig. 2). Aptamer sequences collapsed in Round 4 to two major branches with two overlapping motifs (Motif 1 and 2). In Round 5, a new motif, Motif 3 emerged, as well as Motif 4, which overlaps with Motif 1. Supplementary Table 4 shows the top 20 aptamers identified from round 5 in order of prevalence, the predicted motif, as well as the enrichment of each aptamer in successive rounds.

Five aptamers (named according to their rank in Supplementary Table 4 and listed in Supplementary Table 5) were selected for binding studies with primary T cells and counter selection J.RT3-T3.5 cells based on their abundance, motif, enrichment between rounds, family representation on the phylogenetic tree, and low energy state of their secondary structure (Supplementary Fig. 3). Fluorescein-labeled aptamers A1, A3, and A8 showed specific binding to a subset of mixed T cells whereas A2 and A7 exhibited whole population binding to both T cells and J.RT3-T3.5 cells compared to a randomly chosen aptamer from the naïve library (RN) (Supplementary Fig. 4). Interestingly, A2 and A7, but not A1, A3, and A8, belong to the unique Motif 3 that appeared in round 5 and showed significant enrichment (>100-fold) between rounds 4 and 5 when non-specific binding to J.RT3-T3.5 cells in the bulk aptamer pool was observed.

Characterization of T cell-binding aptamers

We hypothesized that aptamers A1, A3 and A8 likely bind the same receptor due to their overlapping motifs. Furthermore, we suspected that the aptamers bind to CD8 since this protein is not expressed on the counter selection cell line and CD8:CD4 T cell ratios are low in healthy donor pan-T cell isolates, consistent with the 20–30% mixed T cell population binding observed (Supplementary Fig. 4). We therefore analyzed aptamer binding to mixed human T cells with CD4 and CD8 antibody labeling and demonstrated that all three aptamers bind to $CD8^{+}$ but not $CD4^{+}$ T cells, suggesting aptamers bind to human CD8 (Fig. 2a). A similar binding study against murine splenocytes did not, however, show any binding to the T lymphocyte subset, suggesting that the aptamers, like anti-human CD8 antibodies, do not bind murine CD8 (Supplementary Fig. 5a). Aptamers A1, A3, and A8, however, do

bind to $CD8^+$ T cells in rhesus macaque PBMCs, which is consistent with the rhesus cross-reactivity observed in many anti-human CD8 antibody clones (Supplementary Fig. 5b). We validated that these aptamers bind the human CD8 alpha chain isoform (CD8a) expressed on cells by three techniques: competitive binding with a CD8-specific antibody, siRNA knockdown of CD8a in T cells, and enforced CD8a expression in $CD8^-$ cells. Increasing concentrations of an unlabeled CD8-specific antibody (clone RPA-T8), but not a CD3-specific antibody, robustly outcompeted all three aptamers for binding to $CD8^+$ T cells during a co-incubation (Supplementary Fig. 6). CD8a knockdown (75%) by siRNA (Supplementary Table 6) in primary $CD8^+$ T cells was confirmed by antibody staining and correlated with 73–77% reduction in binding of all three aptamers (Fig. 2b). Transient expression of CD8a from a GFP reporter plasmid in $CD8^-$ Jurkat immortalized human lymphocyte cells introduced aptamer binding specifically to GFP^+ cells (Fig. 2c).

For validation of aptamer binding to the CD8a protein itself, we measured association and dissociation kinetics by bio-layer interferometry (BLI), in which a serial dilution of recombinant extracellular CD8a protein (Ser22-Asp182) was screened against aptamers immobilized onto streptavidin-coated BLI sensors. Whereas the RN aptamer negative control exhibited no detectable association with the CD8a protein (data not shown), the A1, A3, and A8 aptamers bound the protein with binding affinities (K_D's) of 20.1±0.2, 14.7±0.1, and 5.59±0.11 nM, respectively (Fig. 2d and Supplementary Table 7). Interestingly, the A3 aptamer had both the highest association (K_{on}) and dissociation (K_{dis}) rate constants of the three aptamers, whereas A8 had the slowest K_{dis}. We also evaluated the "apparent" K_D's of aptamer binding to $CD8^+$ T cells by flow cytometry, and the A1, A3, and A8 aptamers have apparent K_D's of 18.3±4.6, 1.9±0.8 and 2.4±0.9 nM, respectively (Fig. 2e). The observed differences in binding affinity values determined by the two methods is expected. Mass transport limitations not present with BLI but present when staining cells in static wells will favor re-binding and thereby limit dissociation, improving the apparent K_D of the faster dissociating A3 relative to the other aptamers. Furthermore, at saturating concentrations of aptamer where binding advantages stemming from high K_{on}'s are diminished given enough time (i.e. binding at or near steady-state), the A8 aptamer displays increased binding over A3, consistent with the large difference in K_{off} between the two aptamers. Regardless, all three aptamers have high binding affinity to CD8a protein and $CD8^+$ T cells with K_D values comparable to monoclonal antibodies.

Reversing aptamer binding with a complementary oligonucleotide

To achieve traceless cell isolation using an aptamer-based affinity agent, a method to reverse aptamer binding to the cell is needed in the cell recovery step. Aptamer binding can be disrupted by nuclease-mediated degradation of the aptamer,[32, 33] applied force,[34] competitive binding,[35] or denaturing the secondary structure, either through heat[36] or complementary oligonucleotide binding.[37–40] Of these aforementioned methods, complementary oligonucleotide displacement is a preferred method due to its advantages of being gentle (e.g. compared to heat or force) with high yield (e.g. compared to competitive binding) and relatively low cost (e.g. compared to nuclease degradation). We therefore designed a CD8-binding aptamer that could be released from cells by binding with a complementary displacement strand ("reversal agent").

Two major considerations in the design of the selection aptamer and reversal agent design are: first, high-affinity binding to target cells by the selection aptamer; second, rapid disruption of the aptamer secondary structure that is critical for receptor binding by the reversal agent. Accordingly, we chose the A3 aptamer for cell selection, not only due to its low apparent K_D for $CD8^+$ T cells, but also for its high K_{on} and K_{off} for CD8a protein. As multivalent display of the aptamer on a selection medium would potentially mitigate passive cell dissociation since there are aptamers in *cis* to retain cell binding even if a few aptamers dissociate, we rationalized that faster association kinetics would likely be more important for cell isolation. Furthermore, a high K_{off} implies less stable binding, suggesting that strategies to reverse aptamer binding by complementary oligonucleotide displacement may be more successful. We also tested a reported CD8 aptamer from the literature;[41, 42] however, low binding was observed in both the published and our binding conditions (Supplementary Fig. 7). A toehold region was then extended on the 3' end of the original A3 sequence (A3t) to facilitate initiation of cell release by the complementary reversal agent (Fig. 3a and Supplementary Table 5). Toeholds are single-strand sequences that allow for complementary sequence binding and supplanting of pre-paired bases through a method known as strand displacement.[43–47] In this case, the reversal agent would undergo strand displacement via a toehold to abrogate intrastrand base pairing in the aptamer necessary for its secondary structure. Zhang and Winfree report that the rate constant of strand displacement depends critically on the toehold length, varying over up to 6 orders of magnitude, with maximum rates reached with toeholds over 6 bases in length;[47] an 8-mer toehold was therefore used in our CD8-aptamer selection agent. The reversal agent (RA) was designed to be 36 bases in length based on the predicted change in secondary structure upon binding (Fig. 3b and Supplementary Table 5).

We demonstrated effective and rapid aptamer release from cells by the RA using a fluorescently-labeled aptamer with flow cytometry analysis. To determine appropriate conditions for release, various concentrations of RA (ranging from 25–100-fold excess), temperatures (4 ºC, room temperature, and 37 ºC), and times of incubation (5, 10, and 20 min) were evaluated (Supplementary Fig. 8). While >70% A3t aptamer release was observed in all conditions, 90% release could be achieved with just 10 min incubation at room temperature with 100-fold excess RA. Accordingly, we chose these parameters for our label-free isolation strategy.

An aptamer-based strategy for traceless T cell isolation

Prior to applying the A3t aptamer to a cell selection process, it was imperative to ensure that the aptamer selectively binds T cells within the context of PBMCs. At the concentration to be used for cell isolation (5 nM), minimal binding to $CD3^-CD56^-CD14^+$ monocytes and $CD3^-CD56^-CD19^+$ B cells was observed, and binding to these cell populations was not above the RN aptamer control (Supplementary Fig. 9). Binding to B cells was especially low (close to 0%)—a desirable trait given that transduction of a single, highly competent leukemic B cell with a CAR was recently shown to induce resistance to therapy.[48] Besides $CD3^+CD56^-$ T cells, the A3t aptamer also expectedly displayed substantial binding to $CD3^+CD56^+$ NKT cells and $CD3^-CD56^+$ NK cells, which are known to have subsets that express CD8. As NKT cells have been found to improve CAR T cell therapy,[49] binding to

these cells was seen as beneficial. Importantly, the median fluorescent intensity (MFI) of aptamer binding on A3t-positive monocytes, B cells, and NK cells is greatly lower compared to that of A3t-positive T and NKT cells, suggesting that binding events would minimally capture the contaminant cells at this aptamer concentration.

We envisioned that the selection aptamer A3t and its cognate RA could be used to achieve traceless T cell isolation in a completely synthetic system, whereby immobilized aptamers are used to isolate T cells followed by their release by addition of the RA that disrupts the secondary structure of the aptamer critical for binding (Fig. 4a). We tested this strategy using the A3t aptamer immobilized on immunomagnetic Anti-Biotin Microbeads (Miltenyi Biotec). We compared the aptamer strategy to antibody-based CD8 Microbeads (Miltenyi Biotec) for its ability to isolate $CD8^+$ T cells with high purity and yield from three healthy donor PBMC populations, since CD8 Microbeads are currently the only selection technology approved for clinical-scale CAR T cell manufacturing. PBMCs were incubated with functionalized beads and applied onto a column under a magnetic field, after which the flow through (FT) fraction was collected. Whereas antibody-isolated cells were then removed from the column using a column flush (CF), aptamer-isolated cells were exposed to 100-fold excess of RA for 10 min on the column. The column was then unplugged and washed, which constituted the reversal agent elution (RAE) fraction. Any remaining cells on the column were removed using a CF. The fractions of both isolation methods were analyzed via flow cytometry (Supplementary Fig. 10)

We observed near complete depletion of $CD8^+$ cells from the FT fraction using aptamer-loaded microbeads, comparable to the antibody-based CD8 Microbeads, and this corresponded to enrichment of $CD8^+$ cells in the RAE and CF fractions (Fig. 4b). Further analysis of the $CD8^+$ cells in the RAE fraction showed that these cells were predominantly $CD3^+CD16^-$ T cells (>97%), with only a small fraction of the population being $CD8^{lo}CD16^+$ monocytes and NK cells (Fig. 4c). Importantly, this purity analysis is conservative, as it does not account for $CD3^+CD16^+$ NKT cells. On average, the RAE and CF of aptamer-based isolation combined yielded 97.5% of the $CD8^+$ T cells from the starting PBMC population, comparable to antibody-based isolation, and the traceless isolation alone (RAE fraction) yielded 72.3% (Fig. 4d). Even including contaminating $CD8^-$ cells, the average purity of $CD8^+$ T cells in the RAE fraction was 95.6%, illustrating that the A3t aptamer displays minimal non-specific binding to $CD8^-$ cells in PBMCs (Fig. 4e). CD8 staining of aptamer-isolated $CD8^+$ T cells in the RAE fraction with the RPA-T8 antibody clone was comparable to that of $CD8^+$ T cells in the starting PBMC population, whereas that of antibody-isolated $CD8^+$ T cells was lower (Fig. 4f). Given that the antibody-based method depletes nearly the whole $CD8^+$ T cell population (Fig. 4b, d), the lower CD8 staining is likely a result of the cell-bound CD8 Microbeads hindering the binding of the staining antibody clone used (Fig. 4f). This further emphasizes certain advantages of the traceless nature of RA strand displacement, which can enable accurate, downstream phenotyping of capture antigens without needing to optimize the staining antibody clone. Interestingly, aptamer-isolated $CD8^+$ T cells in the CF fraction that were not stripped off in the RAE were just as pure as those in the RAE fraction (Fig. 4e). However, they also had higher CD8 expression than those in the RAE fraction (Fig. 4f), albeit not significantly so, indicating that cells with higher CD8 expression and thus aptamer-bead labeling may be more difficult to

remove from the column by RAE. While simply flushing the column would provide a similarly pure product with higher yield than using a reversal agent, RAE allows isolation of cells free of magnetic beads in a manner that is specific to each selection aptamer used. In addition to providing traceless cell recovery, this approach affords the potential for both further downstream selection of different cell subsets and serial selection of different cell types from a single selection process.

To confirm that aptamer-isolated cells are similar to antibody-isolated cells, we compared the $CD8^+$ T cells in the RAE fraction of aptamer-based isolation to those of antibody-based isolation using flow cytometry phenotyping and NanoString nCounter transcript profiling. Whereas $CD8^+$ T cells in the aptamer-isolated RAE fraction were phenotypically identical to those in PBMCs, antibody-isolated $CD8^+$ T cells comprised of a slightly larger percentage of cells in a transitional stage of dual CD45RA/RO expression which coincided with a small reduction in effector memory cells (Supplementary Fig. 11a). Transcriptionally, however, aptamer- and antibody-isolated cells were identical (Supplementary Fig. 11b). No gene transcripts were differentially expressed largely or significantly, suggesting that there are no immediate side effects to briefly exposing the cells to high RA concentrations.

Generation of CAR T cells from aptamer-based traceless cell isolates

While few differences were observed between aptamer- and antibody-isolated cells immediately after isolation, we sought to confirm if this would stay true for a final CAR T cell product generated using these different isolation methods. We thus generated $CD8^+$ CAR T cells from both the antibody-isolated cells and the traceless aptamer-isolated cells (RAE fraction) shown in Fig. 4d-f and fully compared their outgrowth, phenotype, gene expression, and effector function. Antibody-isolated $CD4^+$ T cells were not included in these studies so as not to convolute any differences between the $CD8^+$ T cells isolated from the different methods. We transduced cells with the PLAT-02 lentiviral vector, which encodes a second generation CD19scFv-41BB-CD3ζ CAR (and a EGFRt surrogate transduction marker) that is used in ongoing clinical trials (Fig. 5a).[9] CD19 CAR T cells were manufactured using a sequential 2-week stimulation bead outgrowth from days S1D0 to S1D14 and 2-week rapid expansion protocol (REP) with irradiated $CD19^+$ feeder cells from days S1R1D0 to S1R1D14, as summarized in Supplementary Fig. 12. After transduction, high expression of the surrogate transduction marker EGFRt (>60%) was observed on S1D9 without additional selection and was further increased using immunomagnetic enrichment and over the REP period to at least 94% on S1R1D13 before functional assays were ran (Fig. 5b). Importantly, while transduction copy number was likely variable, given the variation in surrogate transduction marker expression, there was no difference in the mean EGFRt MFI between antibody- and aptamer-isolated cells (Fig. 5b).

Over the two-week stimulation period, we observed no differences in the outgrowth between untransduced antibody- and aptamer-isolated mock T cells (Fig. 5c). This was consistent with the similar Ki-67 expression between both mocks and CD19 CAR T cells from the different isolation methods at the end of the two-week stimulation outgrowth (Fig. 5d), and unsurprisingly the cells grew identically over REP (Supplementary Fig. 13). Staining on S1D14 for PD1, TIM3, and LAG3 coexpression, markers of both activation and exhaustion,

we observed small differences in accumulation of these markers between cells from the different isolation methods at the end of the two-week stimulation outgrowth (Fig. 5e and Supplementary Fig. 14). Whereas aptamer-isolated CD19 CAR T cells saw loss of $TIM3^{+}PD1^{-}TIM3^{-}$ cells and gain of $PD1^{+}TIM3^{+}$ cells compared to antibody-isolated cells, opposite trends were seen in the mock cells between the two isolation methods, suggesting that these differences are likely artifacts of transduction and the stimulation process and not the isolation strategy. Consistent with the exhaustion/activation data, aptamer-isolated CD19 CAR T cells from the same day exhibited more differentiation than the antibody-isolated cells, as indicated by the greater proportion of $CD45RA^{-}CD62L^{+}$, but the mock cells of the two isolation methods were equivalently differentiated (Fig. 5f, **left** and Supplementary Fig. 15). After a two-week REP process though, the aptamer-isolated CD19 CAR T cells were less terminally differentiated than the antibody-isolated cells while the mocks remained the same, again suggesting that the isolation strategy is not the principal cause of these small differences (Fig. 5f, **right** and Supplementary Fig. 15). NanoString nCounter transcript profiling of immune-associated genes further reaffirmed that there were minimal differences between the two isolation methods with zero genes being greatly or significantly differentially expressed between aptamer- and antibody-isolated mock and CD19 CAR T cells at the end of REP before functional testing (Supplementary Fig. 16). These results reaffirm that the aptamer selections strategy did not have any durable, long-term side effects on CAR T cell fitness.

We evaluated the anti-tumor effector function of these cells against both myelogenous leukemia K562 cells lines that were transduced to stably express OKT3 Fab and CD19 for CD3 and CAR engagement, respectively, as well as B lymphoma Raji cells that constitutively express moderate levels of CD19 (Supplemental Fig. 17). Upon tumor challenge *in vitro*, aptamer-isolated CD19 CAR T cells lysed all three cell types to similar extents as antibody-isolated cells and secreted identical amounts of effector cytokines TNFα and IFNγ (Fig. 5g-h). Thus, CAR T cells derived from an aptamer-based traceless isolation strategy perform *in vitro* to the standard of cells derived from widely used antibody-based isolation.

Aptamer-isolated CAR T cell performance in systemic Raji tumor mouse model

In vitro cytotoxicity results with CAR T cells do not always corroborate with *in vivo* results.[50] Thus, despite observing little differences in the effector function of antibody- and aptamer-isolated $CD8^{+}$ CAR T cells *in vitro*, it was important to further show that this would translate *in vivo*. To this end, we utilized a less stringent version of the previously described CAR T cell stress test,[50, 51] in which Raji-bearing NSG mice were treated with a non-curative dose of $CD8^{+}$ CD19 CAR T cells from the different isolation methods at the end of REP (S1R1D14). Mice were injected with 5×10^{5} GFP-ffluc $CD19^{+}$ Raji cells and treated 7 days later with 10^{7} antibody- or aptamer-isolated S1R1D14 $CD8^{+}$ CAR T cells, as previously described.[52] $CD8^{+}$ mock T cells from both isolation methods were included as placebo controls.

Administration of 2×10^{7} $CD8^{+}$ CAR T cells was previously shown to be only 50% curative long-term with this model due to lacking the $CD4^{+}$ CAR T cell subset critical for therapy

persistance.[52] The $CD8^+$ CAR T cells in this study were also expanded by both a 2-week bead stimulation and 2-week REP, and thus displayed markedly more exhaustion and differentiation than 1-week or 2-week expanded CAR T cells described in other publications.[50, 51] Consequently, unpublished work using only 10^7 $CD8^+$ CD19 CAR T cells in the same model was found to be non-curative with a maximal survival of approximately 10-weeks. We therefore postulated that this T cell stress study design would be able to rigorously identify any differences in anti-tumor effector function between antibody- and aptamer-isolated CAR T cells. Even so, *in vivo*, we continued to observe identical anti-tumor activity between both antibody- and aptamer-isolated $CD8^+$ CAR T cells. Tumor regression and relapse kinetics, as measured by photon flux of the tumor, overlapped between mice that received CAR T cells derived from the different isolation methods across multiple donors. (Fig. 6a). While the therapy was non-curative for both CAR T cell treatment groups, indicative of a successful stress test model, mice receiving aptamer-isolated CAR T cells exhibited similar prolonged survival compared to mice receiving antibody-isolated CAR T cells, as determined by both biological significance (median survival time) and log-rank statistical significance (Fig. 6b). These results further illustrate that traceless aptamer-based cell isolation with strand displacement is a viable replacement for antibody-based isolation in the initial production step of CAR T cell therapy, having negligible, downstream impact on the quality of the final cell product.

DISCUSSION

A challenge with CAR-T cell therapy is the time and cost associated with manufacturing a clinical product. As recent literature has shown that selection of different T-cell subsets for therapy may provide improved and consistent clinical outcomes compared to undefined products starting from heterogenous PBMCs, it is increasingly imperative that efficient and cost-effective selection approaches are developed to meet the demands of these new therapeutic compositions.[7, 8] Currently, $CD8^+$ and $CD4^+$ T cells are selected by either (i) splitting the starting leukapheresis product and immunomagnetically depleting undesired cells for further downstream positive selections or (ii) sequentially isolating from the leukapheresis product using immunomagnetic positive selections. Both approaches are far from perfect: the former wastes a portion of the cells in the starting population by nature of splitting the cells but saves time with parallel isolations, while the latter is time consuming by using the whole population in each step. Furthermore, remaining labels on the cells prevent further selection and present regulatory barriers for clinical translation into patients. Two recent reports have used DNA-labeled antibodies followed by strand displacement to isolate multiple cell populations; however, antibodies and DNA tags remain attached to selected cells.[53, 54] The advent of Streptamer technology and similar avidity-reliant Fab multimerization strategies have partially mitigated these issues by enabling label-free isolation; however, these approaches still rely on expensive, biologically-produced selection agents and require two or more apparatuses in sequence to isolate pure, separate cell subsets.[16, 17] Additionally, these technologies are perishable and frequently have a sole supplier of consumables, which adds supply-chain risk to a cell therapy manufacturing process that is often time-sensitive for the patients with refractory disease.[10]

DNA aptamers and complementary strand displacement with a reversal agent present a unique opportunity to improve selection of T cells for use in adoptive cell therapy. Aptamers are synthetic and thereby inexpensive to produce at large scales. Furthermore, their manufacturing can be outsourced to one of many available companies. Added with their long-shelf life, they bear minimal supply-chain risk. High-affinity DNA aptamers can be developed against multiple targets and their sequences can be further modified post-SELEX to include unique toeholds and stems for aptamer-specific strand displacement. Thus, panels of aptamers against diverse T cell antigens can be developed with corresponding unique reversal agents for sequential label-free isolation of different cell subsets off the same column. As an example, microbeads loaded with CD4 and CD8 aptamers that have unique toeholds and sequences could be added at the same time to one whole leukapheresis product, and $CD4^+$ and $CD8^+$ T cells could be serially eluted off one column by sequential incubations with the corresponding reversal agents. A similar outcome can be achieved using a CD3 aptamer in combination with either a CD4 or CD8 aptamer. Alternatively, one could deplete $CD8^+$ T cells and other unwanted cell subsets using a CD8-specific aptamer and other aptamers that bind monocytes, B cells, and NK cells, respectively. Untouched $CD4^+$ T cells could then be enriched in the flow through fraction, and $CD8^+$ T cells could be selectively eluted from the column using a reversal agent specific to the CD8 aptamer. The key to executing these strategies is the identification of highly cell-specific aptamers.

In this study, we report the discovery of high-affinity CD8a-specific aptamers and the successful application of one aptamer with a reversal agent in a traceless $CD8^+$ T cell isolation system. With the aptamer alone, we report equivalent $CD8^+$ T cell selection yield compared to a widely-used antibody-based approach. With a reversal agent for label-free elution, we observed >70% selection yield and >95% purity of $CD8^+$ T cells. Given that a 350–450 mL apheresis product from an ALL patient will have 3–9 × 10^9 T cells, and only 200–600 × 10^6 $CD8^+$ T cells are needed to manufacture a 1:1 $CD4^+$:$CD8^+$ CAR T cell therapy, the trade of lower yield for high purity, lower cost, and label-free selection with this approach has little consequence but many benefits. Importantly, based on anecdotal observations of the maximal capacity of this system at a small scale, we estimate that only $5–10 of aptamer would be needed for reliable clinical-scale isolation. CD19-directed CAR T cells manufactured from label-free, aptamer-isolated cells also exhibited identical performance as CAR T cells generated from antibody-selected cells in assays designed to measure anti-tumor effector function, showing that aptamer-based traceless cell isolation is a practical selection strategy for CAR T cell therapy.

Although the competitive SELEX approach was designed to identify multiple T cell-specific aptamers, only CD8-specific aptamers were discovered with this strategy. We speculate that this occurred due to the strong partitioning of the library towards the high-affinity CD8 aptamers. SELEX strategies using untouched $CD4^+$ primary T cells or the $CD8^-$ Jurkat T cell line may thus be required to identify aptamers that bind to alternative T cell antigens like CD3 or CD4. Furthermore, due to the limited binding chemistry available to unmodified DNA aptamers, certain proteins may not be amenable to high-affinity aptamer discovery using unmodified DNA libraries. For these targets, increased chemical diversity by including one or two modified base pairs in the library design may be needed for the successful partitioning of high-affinity binders.[55]

In future, aptamers could be readily functionalized for attachment to solid supports for affinity chromatography separation, thus resulting in a purely synthetic isolation system without the need for recombinant proteins, magnetic supports, and pre-incubation with selection agents. Cell-release efficiency could be potentially improved, such as by refining the strand displacement kinetics between aptamer and reversal agent through further sequence optimization (higher toehold GC content, aptamer truncation) and chemical modification of the aptamer and reversal agent (locked nucleic acids).[47, 56] Further discovery of aptamers against the T-cell markers CD3 and CD4 will also be required to realize a serial selection strategy that can isolate multiple cell subsets tracelessly from a single column. With these advances, aptamer and reversal agent-based isolation approaches could be inexpensively applied in process-engineering strategies to prepare engineered $CD4^+$ and $CD8^+$ T cells through continuous flow methods, thus increasing the accessibility of T cell immunotherapy.

METHODS

Oligonucleotides.

All oligonucleotides studied were synthesized by Integrated DNA Technologies. The ssDNA library used in the T cell SELEX process was HPLC purified and consisted of a 52-base pair (bp) random sequence flanked by two 18-bp constant regions. The primers used for library amplification between SELEX rounds, with IDT modification codes, are as follows: forward 5'-/56-FAM/ATCCAGAGTGACGCAGCA-3' and reverse 5'-/5BiosG/ACTAAGCCACCGTGTCCA-3'. The individually synthesized ssDNA aptamers are listed in Supplementary Table 5.

Antibodies and flow cytometry.

The following dyes, antibodies, and secondaries were used to stain cells: Zombie Violet (1:500 in 100 μL/10^6 cells, BioLegend), Zombie Yellow (1:500 in 100 μL/10^6 cells, BioLegend), APC anti-human CD4 (1:100, 300514, BioLegend), PerCP/Cy5.5 anti-human CD8a (1:100, 301031, BioLegend), APC anti-human CD8a (rhesus cross-reactivity, 1:100, 301014, BioLegend), CD8-biotin (1:100, 130–098-556, Miltenyi), anti-mouse CD16/CD32 Fc block (1:100, 14–0161-86, eBioscience), FITC anti-mouse CD3e (1:50, 100305, BioLegend), BV421 anti-mouse CD8a (1:50, 100737, BioLegend), FITC mouse anti-human CD3e (rhesus cross-reactivity, 1:20, 55611, BD Biosciences), Purified anti-human CD3 (Clone UCHT1, 300402, BioLegend), Purified anti-human CD8a (Clone RPA-T8, 301002, BioLegend), Super Bright 600 anti-human CD19 (1:20, 63–0198-42, eBioscience), Super Bright 702 anti-human CD56 (1:100, 67–0566-42, eBioscience), PE anti-human CD3 (1:100, 300308, BioLegend), APC/Cy7 anti-human CD14 (1:40, 325619, BioLegend), FITC anti-human CD16 (1:50, 302006, BioLegend), Alexa Fluor 700 anti-human CD3 (1:50, 300424, BioLegend), Brilliant Violet 785 anti-human CD4 (1:50, 317442, BioLegend), PE/Cy7 anti-human CD8a (1:200, 300914, BioLegend), BUV737 mouse anti-human CD45RA (1:25, 564442, BD Biosciences), BUV395 mouse anti-human CD45RO (1:25, 564291, BD Biosciences), PE anti-human CD62L (1:400, 304806, BioLegend), Brilliant Violet 421 anti-human CCR7 (1:25, 353208, BioLegend), Erbitux-biotin (1:500, Jensen Lab), PE-Cy7 mouse anti-Ki-67 (1:20, 561283, BD Biosciences), BUV737 mouse anti-

human PD-1 (1:20, 565299, BD Biosciences), Brilliant Violet 785 anti-human TIM-3 (1:20, 345032, BioLegend), PE mouse anti-human LAG-3 (1:20, 565616, BD Biosciences), Brilliant Violet 785 anti-human CD45RA (1:160, 304140, BioLegend), NeutrAvidin Protein DyLight 633 (1:500, 22844, Invitrogen), Alexa Fluor 647 Streptavidin (1:500, 405237, BioLegend), and PE Streptavidin (1:500, 405204, BioLegend). OneComp eBeads (Invitrogen) were used to prepare single-color controls for compensation, if needed. Stained samples were analyzed with either a MACSQuant Analyzer 10 (Miltenyi), Attune NxT (Invitrogen), or BD LSRFortessa (BD Biosciences) flow cytometer.

Cell line culture and PBMC isolation.

J.RT3-T3.5 and Jurkat (Clone E6–1) cell lines used for counter selection and nucleofection, respectively, were purchased from ATCC. The Epstein-Barr virus transformed lymphoblastoid cell line (TM-LCL) used in the rapid expansion protocol (REP) of T cells was made from mononuclear cells as previously described.[57] $CD19^+$ and $OKT3^+$ K562 cells used for functional assays were generated by lentivirally transducing parental K562 parental cells (ATCC) with CD19- or OKT3-expressing constructs. Raji parental cells were also purchased from ATCC. All the above cell lines were cultured in RPMI 1640 medium (Gibco) with 10% heat-inactivated FBS (Life Tech and VWR). Human peripheral blood mononuclear cells (PBMCs) were isolated from Leukocyte Reduction System (LRS) cones (Bloodworks Northwest) using Ficoll-Paque density gradient centrifugation (GE). Mixed or $CD8^+$ T cells used in non-isolation experiments were a generous gift from Juno Therapeutics. Rhesus PBMCs were a generous gift from Dr. Agne Taraseviciute (Seattle Children's Research Institute).

Competitive cell SELEX with T cell depletion.

The SELEX protocol was adapted from a reported method.[28] A schematic of the SELEX procedure is shown in Fig. 1, and the conditions used in the individual rounds are summarized in Supplementary Table 2. Broadly, positive selection was conducted for Round 1, in which 4×10^7 thawed mixed T cells, depleted of dead cells (Miltenyi), were incubated with 40 nmol ssDNA library (~10^{16} individual sequences) for 1 h at 4 °C in binding buffer. Bound aptamers were extracted and amplified by PCR using Phusion High Fidelity DNA Polymerize (NEB) with forward and reverse primers. Strand separation was performed with High Capacity Neutravidin Agarose Resin (Thermo Scientific), as described previously,[28] and the FAM-labeled ssDNA aptamer pool was used in next round. For Rounds 2–5, the ssDNA aptamer pools were incubated with thawed PBMCs depleted of dead cells, a process termed competitive selection. After three washes, T cells and bound ssDNA sequences were then enriched using a Pan T Cell Isolation Kit (Miltenyi). The ssDNA pool was then extracted and incubated with 10^7 $CD3^-CD8^-$ J.RT3-T3.5 cells at 4 °C as a form of negative selection in each round, and unbound ssDNA sequences were PCR amplified and used to generate ssDNA aptamer pools for use in the sequential round. The wash and binding buffer formulations, as well as folding conditions, are as described previously.[28]

Aptamer binding assays.

Cells (2×10^5) were incubated with 100 μL folded FAM-labeled ssDNA pools or FAM/biotin-labeled individual aptamers for 20–30 min at 4 °C in binding buffer at the indicated

concentrations. For antibody competition and multi-color flow cytometry staining with antibodies, antibodies were added in to the primary incubation with aptamer. Cells were washed twice (or three times for large flow panels) in 200 μL wash buffer supplemented with 1% BSA to remove excess aptamer. If the aptamers or antibodies used were biotinylated, cells underwent a second incubation with 100 μL fluorescently-labeled streptavidin or neutravidin secondary for 15–20 min at 4 °C in wash buffer with 1% BSA and washed twice. Stained cells were fixed in 200 μL wash buffer with 1% BSA and 0.1% PFA before analyzing via flow cytometry.

Next generation sequencing and data analysis.

The starting naive library and ssDNA pools from each SELEX round were PCR amplified with barcoded primers listed in Supplementary Table 3 for sequencing using the MiSeq Reagent Kit v2 (300 cycles) and MiSeq System (Illumina) according to the manufacturer's instructions. Exported FASTA files were analyzed with FASTAptamer software.[29] Specifically, *FASTAptamer-Count* was first used to determine rank and reads per million (RPM) for each sequence, where after *FASTAptamer-Compare* was used to conduct pairwise comparison of RPM of sequences between adjacent rounds and thus calculated fold enrichment (Supplementary Table 4). Neighbor joining trees were constructed for the top top 100 sequences from Rounds 2–4 and were further analyzed by both FigTree software (tree.bio.ed.ac.uk/software/figtree/) for phylogenetic tree generation and MEME Suite software for motif prediction.[31] The NUPACK web application was used to generate predicted secondary structures of aptamer sequences.[58]

Murine splenocyte isolation and staining.

For mouse spleen harvesting, animal work was conducted under protocol number 4053–01 approved by the Institutional Animal Care and Use Committee (IACUC) at the University of Washington. 20-week-old Tg(Aldh1l1-EGFP,-DTA)D8Rth/J male mice (Jackson Laboratory) were euthanized with avertin and perfused with 20 mL PBS to limit coagulation.[59] Spleens were harvested, minced with scissors, and dissociated by sieving over a 40-μm cell strainer (Falcon). Red blood cells (RBCs) were removed by incubation with ACK Lysing Buffer (Gibco) and cells were stained with both anti-mCD3 and anti-mCD8 antibodies and aptamers.

siRNA knockdown.

10^7 thawed $CD8^+$ T cells were activated with Dynabeads Human T-activator CD3/CD28 (Life Tech) at 1.5×10^6 cells/mL for 3 days in complete RPMI supplemented with 100 U/mL rhIL-2 (Miltenyi, NIBSC calibrated value). On day 3, 3×10^6 activated T cells were nucleofected with 50 pmol of both CD8a-targetting duplex siRNA (DsiRNA) 1 and 2, listed in Supplementary Table 6, or 100 pmol of scrambled DsiRNA (IDT) using the Human T Cell Nucleofector Kit (Lonza) with Program T-023 according to the manufacturer's instructions. Aptamer and anti-CD8 antibody staining, as discussed in the previous section, was performed 24 h later and analyzed via flow cytometry.

Plasmid transfection.

CD8a-hnRNP-M-EGFP was a gift from Lei Lu (Addgene plasmid # 86054).[60] 2×10^6 $CD8^-$ Jurkat cells were nucleofected (Lonza) with 2 μg of the plasmid using the Nucleofector Kit V (Lonza) with Program X-001 according to the manufacturer's instructions. The cells were analyzed 24 h later for both GFP expression and anti-CD8 antibody and aptamer binding via flow cytometry.

Bio-layer interferometry.

BLI studies were conducted on a FortéBio Octet Red96 instrument at 25 °C with sample agitation at 1000 rpm. The sample buffer used for all steps was comprised of binding buffer with 0.01% tween-20. Streptavidin-coated biosensors were loaded with 50nM biotinylated aptamer until all sensors (except for the reference) reached a capture threshold of 0.5 nm. After a 100 sec rinse and baseline steps in buffer alone, sensors were exposed to a 1:3 dilution series of recombinant human CD8a protein (Sino Biological) ranging from 150nM to 5.56nM. Association with protein was monitored for 1200 sec, and dissociation was carried out for 600 sec in buffer alone. Data analysis was carried out using Octet Data Analysis 9.0 software (FortéBio). Kinetic constants were calculated by conducting a global fit of the several processed association and dissociation curves from the protein dilution series to a 1:1 binding model. The quality of the fit was evaluated by the R^2 and χ^2 values.

Comparison to previously reported aptamer.

CD8Ap17s, as described by Wang *et al.*, was synthesized with the sequence 5'-CTACAGCTTGCTATGCTCCCCTTGGGGTA/iSp18//3Bio/−3'.[42] Binding to $CD8^+$ T cells was compared to our aptamer A3t (Supplementary Table 5), except CD8Ap17s binding buffer (A-BB) and folding conditions were also used in addition to our binding buffer (T-BB) and folding conditions. For the CD8Ap17s conditions, 1 μM of each aptamer was folded by denaturation at 95 °C for 5 min and cooling to 37 °C in their wash buffer (40mM HEPES, 150mM NaCl, 5mM KCl, 1mM $MgCl_2$, 1mM $CaCl_2$, pH 7.5). Binding was similarly carried out and analyzed as detailed above but in CD8Ap17s binding buffer, which comprised of the wash buffer supplemented with 5% FBS.

Reversal agent optimization.

A 36-bp reversal agent was designed complementary to the 3' end of aptamer A3t (Supplementary Table 5). Binding to $CD8^+$ T cells with 5nM aptamer A3t was first carried out with secondary fluorescent streptavidin labeling, as discussed above. Labeled cells were then incubated with varying fold-excess (over the amount of aptamer used) of 200 μL reversal agent in wash buffer with 1% BSA for different times and temperatures. Cells were washed twice with wash buffer 1% BSA to remove eluted aptamers, fixed, and analyzed via flow cytometry.

Traceless selection of $CD8^+$ T cells from PBMC.

For each PBMC donor, 200 μL of Anti-Biotin Microbeads (Miltenyi) were diluted to 1000 μL in binding buffer with 5 nM aptamer A3t and incubated for 15 min at 4 °C under gentle rotation. The aptamer-labeled bead suspensions were then added to 2×10^8 Ficoll-isolated

PBMCs and allowed to incubate for another 15 min at 4 °C under gentle rotation. Cells were subsequently washed with 10 mL autoMACS Rinsing Solution (Miltenyi) supplemented with 0.5% BSA, resuspended in the same buffer, and applied over two LS Columns in parallel on a QuadroMACS separator (Miltenyi) per the manufacturer's instructions. A flow through (FT) fraction, which includes the flow through from the initial application of cells and the three subsequent 3mL column washes, was collected. Afterwards, 1 mL of 500nM reversal agent (100-fold excess) in autoMACS solution with 0.5% BSA and 5mM MgCl2 was applied to the column on the magnet containing cells labeled with aptamer-functionalized microbeads. Approximately 600–700 μL of the reversal agent solution passed through the column before it was plugged with a M/F Luer Lock Plug (Smiths Medical) for a 10 min incubation at room temperature. Upon removal of the plug, the column was washed three times with 3mL autoMACS solution with 0.5% BSA and 5mM EDTA, which constituted the reversal agent elution (RAE) fraction. The RAE cells were immediately spun down and resuspended in fresh buffer to remove any reversal agent. Remaining cells on the column were removed with a column flush (CF) per the manufacturer's instructions. In parallel, $CD8^+$ cells from the same donor were also isolated from 200×10^6 PBMCs in the CF fraction with antibody-based CD8 Microbeads (Miltenyi), according to the manufacturer's instructions.

All fractions were counted and analyzed via flow cytometry with two antibody panels: (i) a yield panel staining for CD3, CD8, and CD16 expression and (ii) a phenotype panel staining for CD3, CD4, CD8, CD45RA, CD45RO, CCR7, and CD62L expression. Furthermore, 10^6 cell pellets from both the antibody-isolated CF fraction and aptamer-isolated RAE fraction were flash frozen on dry ice and ethanol for NanoString nCounter analysis. Remaining cells were banked for downstream CAR T cell production.

CD19 CAR T cell manufacturing.

$CD8^+$ T cells of both isolation methods from each donor were thawed and 3.3×10^6 cells for both mock and CD19 CAR T cell groups were stimulated 1:1 with Dynabeads Human T-Activator CD3/CD28 (Invitrogen) in 4 mL complete RPMI with 50 U/μL rhIL-2 (Miltenyi) and 0.5 ng/mL rhIL-15 (Miltenyi) in a 12-well plate. After two days (S1D2), cells designated for CAR T cell production were transduced with clinical-grade PLAT-02 CD19 CAR lentiviral vector (a gift from the City of Hope) at a multiplicity of infection (MOI) of 0.3 with 40 μg/mL protamine sulfate via spinoculation for 30 min at 800xg at 32 °C. Thereafter, media exchanges were conducted every 2–3 days to replenish cytokines, and cells were moved to larger culture vessels when cell concentrations reached $1.5–2 \times 10^6$ cells/mL. The activator beads were removed 9-days post-stimulation, termed S1D9, and cells were stained for EGFRt surrogate marker expression to assess transduction efficiency. CAR^+ cells were magnetically enriched 12-days post-stimulation (S1D12) using biotinylated Erbitux antibody and Anti-Biotin Microbeads per the manufacturer's instructions. On day 14 post-stimulation (S1D14), cells were analyzed via flow cytometry by staining for (i) activation/proliferation with Ki-67, (ii) exhaustion/activation with PD1, TIM3, and LAG3, and (iii) differentiation with CD62L and CD45RA.

The 2-week stimulated T cells were further expanded using a 2-week rapid expansion protocol (REP), as previously described.[61] Briefly, 1.5×10^6 CD19 CAR T cells were co-incubated with 10.5×10^6 irradiated $CD19^+$ TM-LCL feeder cells in 25 mL complete RPMI supplemented with the aforementioned cytokine concentrations in T-25 flasks (Corning). Similarly, 1.5×10^6 mock T cells were co-incubated with 10×10^6 irradiated $CD19^+$ TM-LCL feeder cells and 50×10^6 irradiated donor-mismatched PBMC feeder cells in 25 mL complete RPMI supplemented with the same cytokines and 30 ng/mL OKT3 in T-25 flasks (Corning). PBMCs and TM-LCL cells were irradiated at 3500 and 8000 rads, respectively, using a Cesium source irradiator. Cells were maintained as was done over the 2-week activator bead expansion, except OKT3 was replaced only on Day 2. On day 13 post-REP (S1R1D13), the CD19 CAR T cells were stained for EGFRt surrogate transduction marker expression to assess enrichment and purity of CAR^+ cells after magnetic selection and REP. On day 14 post-REP (S1R1D14), cells were characterized again for differentiation and a 10^6 cell pellet of each cell lot was flash frozen for downstream NanoString nCounter analysis. The remaining cells were used for *in vitro* functional assays or banked for *in vivo* studies.

NanoString nCounter gene profiling.

Thawed cell pellets were resuspended in RLT lysis buffer with β-mercaptoethanol at 3,500 cells/μL, and overnight hybridization reactions with the nCounter Immunology Panel (Human V2) Reporter CodeSet and Capture ProbeSet were ran according to the manufacturer's instructions. Samples were run on the nCounter SPRINT Profiler (NanoString), and mRNA counts were normalized in groups by day and cell type (D0, S1R1D14 mocks, S1R1D14 CD19 CAR) using nSolver 4.0 software (NanoString) and the Advanced Analysis 2.0 software (NanoString), which selects the housekeeping genes that minimize the pairwise variation statistic. Each group has 6 samples, 3 biological replicates for antibody-based isolation and 3 biological replicates for aptamer-based isolation. Using Excel (Microsoft), mRNA probes that gave normalized counts less than 25 for more than 50% of the samples in a group (i.e. 4 or more samples) were removed from the analysis due to being mostly below background. The unadjusted *P*-values of the LOG_2 fold changes in the probe counts of aptamer-isolated cells over antibody-isolated cells were determined using a paired two-tailed t-test in Excel, and the threshold for significance was calculated using the Benjamini-Yekutieli multiple-testing correction in R software.

Anti-tumor cytotoxicity assay.

K562 + OKT3, K562 + CD19, and Raji parental target cells were each seeded at 5×10^6 cells in 4 mL complete RPMI in a well of a 12-well plate, and 75 μL Cr-51 (PerkinElmer) was added to each well with cells. Cells were harvested a day later and seeded at 5×10^3 cells/well in a 96-well plate at 100 μL. S1R1D14 $CD8^+$ mock and CD19 CAR effector T cells in 100 μL were added to the target cells at different effector-to-target (E:T) ratios ranging from 1:1 to 30:1. Media without cells or with 2% SDS were also added to wells with target cells as minimum and maximum lysis controls, respectively. Target and effector cell mixtures were lightly pelleted at 700 rpm for 2 min before incubating for 4 hr at 37 °C in an incubator. 50 μL of supernatant was then harvested into LUMA plates (PerkinElmer) and allowed to dry overnight. The plates were analyzed by a TopCount NXT Microplate Scintillation and Luminescence Counter (PerkinElmer).

Anti-tumor cytokine release assay.

K562 + OKT3, K562 + CD19, and Raji parental target cells were plated at 5×10^4 cells/well in a 96-well plate at 100 μL. S1R1D14 $CD8^+$ mock and CD19 CAR effector T cells were added to target cells at 10^5 cells/well in 100 μL and allowed to co-incubate for 24 h. Cells were then pelleted at 1200 rpm for 3 min, and 120 μL of supernatant was collected and frozen at −80 °C until ready to analyze. Thawed supernatants were diluted 1:5 or 1:20 in RPMI without FBS, and IL-2, IFNγ, and TNFα in the supernatants and a standard (Bio-Rad) were captured and fluorescently detected on magnetic beads using a 3-plex Bio-Plex custom kit with flat magnetic plates (Bio-Rad) according to the manufacturer's instructions. The beads with captured cytokines were analyzed using a Bio-Plex 200 system (Bio-Rad).

T cell stress test mouse model.

All animal work described herein complied with local animal ethical and welfare standards. The T cell stress test mouse model was conducted under protocol number 13853 approved by the IACUC at the Seattle Children's Research Institute. 9- to 11-week-old NOD/SCID/IL-2Rγ null (NSG) female mice (Jackson Laboratory) were inoculated with 5×10^5 GFP-ffluc Raji cells in 200 μL PBS by tail vein injection, followed by 10^7 S1R1D14 antibody- or aptamer-isolated $CD8^+$ mock or CD19 CAR T cells 7 days later. The same three donors from the *in vitro* studies were tested, and for each of the four T cell populations evaluated, 3 mice were used per donor (for a total of 9 mice in each treatment group across all donors). For bioluminescence imaging, mice were injected subcutaneously with 150 μL D-luciferin (PerkinElmer) in PBS (4.29 mg per mouse) and unsaturated images were acquired with the Xenogen IVIS Imaging System (PerkinElmer) after 7 and 10 min using medium or small binning and an acquisition time of 30 sec to 1 min. Photon flux was analyzed using the Living Image software (PerkinElmer). On day 6 post-tumor inoculation, mice were arranged into groups of 3 mice each for each donor and treatment group such that the average photon flux of the pre-established systemic tumors was approximately equal across all groups. Accordingly, no randomization or blinding methods were used. Mice that developed hind-limb paralysis were euthanized by carbon dioxide. The log-rank test was performed using Prism 7.0 software (GraphPad).

Statistical analysis.

Data are expressed as mean ± s.d., unless otherwise stated, and the number of biological and technical replicates is indicated in the figure caption. If only two populations were being compared, a two-tailed t-test was used for hypothesis testing; otherwise, Analysis of Variance or ANOVA was used for hypothesis testing when more than two populations were being compared. Paired hypothesis testing was often implemented to account for large donor-to-donor variability. When conducting multiple comparisons, Tukey's or Dunnett's test was used to adjust *P*-values when every mean was compared to every other mean or a control mean, respectively, whereas the Sidak correction was used to adjust *P*-values when select sets of means were compared, assuming independence. If comparisons could not be assumed to be independent from each other, Bonferroni correction was used instead of the Sidak correction to adjust *P*-values. The Benjamini-Yekutieli correction was used for analysis of NanoString data, as this method handles the dependence between the expression

of different genes well. Differences were considered significant if $P < 0.05$ after any adjustment. Graphing and statistical tests were performed using Prism 7.0 software (GraphPad) unless otherwise stated.

Life Sciences Reporting Summary.

Further information on experimental design is available in the Life Sciences Reporting Summary.

Data availability.

The data that support the main findings of this study are available within the paper and its Supplementary Information. All source data generated for this study and relevant information are available from the corresponding authors upon reasonable request. The NanoString nCounter data have been deposited in the NCBI Gene Expression Omnibus (GEO), with accession code GSE130185.

Supplementary Material

Refer to Web version on PubMed Central for supplementary material.

ACKNOWLEDGEMENTS

This work was supported by a sponsored research agreement from Juno Therapeutics. We are grateful to C. Ramsborg (Juno Therapeutics), Allison Bianchi (Juno Therapeutics), Julie Shi (Juno Therapeutics), Calvin Chan (Juno Therapeutics), B. Olden (University of Washington), and J. Gustafson (Seattle Children's Research Institute) for their critical discussion and helpful advice and to A. Mills (Juno Therapeutics) for manuscript feedback. We are also grateful to all Pun and Jensen Lab members, especially J. Yokoyama (Seattle Children's Research Institute) and A. Johnson (Seattle Children's Research Institute), for experimental support and helpful advice. We also thank the Baker Lab, especially Bobby Langan, for assistance with Octet BLI studies. We also thank C. Saxby (University of Washington) and R. Mukherjee (Seattle Children's Research Institute) for their valuable input on NGS sequencing and NanoString nCounter analysis, respectively. We also thank M. Meechan (Seattle Children's Research Institute) for assisting with mouse bioluminescence imaging and cage monitoring. We also thank members of the Statistical Consulting Program in the Departments of Biostatistics and Statistics, especially T. Hee Wai (University of Washington), for their valuable input on statistical analysis. We also thank H.Y. Lin for preparing the SELEX and cell isolation figures. I. Cardle was supported partly by the National Cancer Institute of the National Institutes of Health under award number 5T32CA080416–19 for research reported in this publication.

REFERENCES

1. Brentjens RJ et al. CD19-targeted T cells rapidly induce molecular remissions in adults with chemotherapy-refractory acute lymphoblastic leukemia. Sci. Transl. Med. 5, 177ra138 (2013).
2. Davila ML et al. Efficacy and toxicity management of 19–28z CAR T cell therapy in B cell acute lymphoblastic leukemia. Sci. Transl. Med. 6, 224ra225 (2014).
3. Lee DW et al. T cells expressing CD19 chimeric antigen receptors for acute lymphoblastic leukaemia in children and young adults: a phase 1 dose-escalation trial. Lancet 385, 517–528 (2015). [PubMed: 25319501]
4. Mirzaei HR, Rodriguez A, Shepphird J, Brown CE & Badie B Chimeric Antigen Receptors T Cell Therapy in Solid Tumor: Challenges and Clinical Applications. Front. Immunol. 8, 1850 (2017). [PubMed: 29312333]
5. Hale M et al. Engineering HIV-Resistant, Anti-HIV Chimeric Antigen Receptor T Cells. Mol. Ther. 25, 570–579 (2017). [PubMed: 28143740]
6. Scholler J et al. Decade-long safety and function of retroviral-modified chimeric antigen receptor T cells. Sci. Transl. Med. 4, 132ra153 (2012).

7. Sommermeyer D et al. Chimeric antigen receptor-modified T cells derived from defined CD8+ and CD4+ subsets confer superior antitumor reactivity in vivo. Leukemia 30, 492–500 (2016). [PubMed: 26369987]
8. Turtle CJ et al. CD19 CAR–T cells of defined CD4+: CD8+ composition in adult B cell ALL patients. J. Clin. Invest. 126, 2123 (2016). [PubMed: 27111235]
9. Gardner RA et al. Intent-to-treat leukemia remission by CD19 CAR T cells of defined formulation and dose in children and young adults. Blood 129, 3322–3331 (2017). [PubMed: 28408462]
10. Aijaz A et al. Biomanufacturing for clinically advanced cell therapies. Nat. Biomed. Eng. 2, 362–376 (2018). [PubMed: 31011198]
11. Terakura S et al. Generation of CD19-chimeric antigen receptor modified CD8+ T cells derived from virus-specific central memory T cells. Blood 119, 72–82 (2012). [PubMed: 22031866]
12. Wang X et al. Phenotypic and functional attributes of lentivirus-modified CD19-specific human CD8+ central memory T cells manufactured at clinical scale. J. Immunother. 35, 689–701 (2012). [PubMed: 23090078]
13. Voss S & Skerra A Mutagenesis of a flexible loop in streptavidin leads to higher affinity for the Strep-tag II peptide and improved performance in recombinant protein purification. Protein Eng. 10, 975–982 (1997). [PubMed: 9415448]
14. Knabel M et al. Reversible MHC multimer staining for functional isolation of T-cell populations and effective adoptive transfer. Nat. Med. 8, 631–637 (2002). [PubMed: 12042816]
15. Schmitt A et al. Adoptive transfer and selective reconstitution of streptamer-selected cytomegalovirus-specific CD8+ T cells leads to virus clearance in patients after allogeneic peripheral blood stem cell transplantation. Transfusion 51, 591–599 (2011). [PubMed: 21133926]
16. Stemberger C et al. Novel serial positive enrichment technology enables clinical multiparameter cell sorting. PLoS One 7, e35798 (2012). [PubMed: 22545138]
17. Sabatino M et al. Generation of clinical-grade CD19-specific CAR-modified CD8+ memory stem cells for the treatment of human B-cell malignancies. Blood 128, 519–528 (2016). [PubMed: 27226436]
18. Ellington AD & Szostak JW In vitro selection of RNA molecules that bind specific ligands. Nature 346, 818 (1990). [PubMed: 1697402]
19. Tuerk C & Gold L Systematic evolution of ligands by exponential enrichment: RNA ligands to bacteriophage T4 DNA polymerase. Science 249, 505–510 (1990). [PubMed: 2200121]
20. Robertson DL & Joyce GF Selection in vitro of an RNA enzyme that specifically cleaves single-stranded DNA. Nature 344, 467 (1990). [PubMed: 1690861]
21. Bunka DH & Stockley PG Aptamers come of age - at last. Nat. Rev. Microbiol. 4, 588–596 (2006). [PubMed: 16845429]
22. Hernandez LI, Machado I, Schafer T & Hernandez FJ Aptamers overview: selection, features and applications. Curr. Top. Med. Chem. 15, 1066–1081 (2015). [PubMed: 25866270]
23. Zhou J & Rossi J Aptamers as targeted therapeutics: current potential and challenges. Nat. Rev. Drug Discov. 16, 181–202 (2017). [PubMed: 27807347]
24. Dunn MR, Jimenez RM & Chaput JC Analysis of aptamer discovery and technology. Nat. Rev. Chem. 1, 0076 (2017).
25. Daniels DA, Chen H, Hicke BJ, Swiderek KM & Gold L A tenascin-C aptamer identified by tumor cell SELEX: systematic evolution of ligands by exponential enrichment. Proc. Natl. Acad. Sci. U. S. A. 100, 15416–15421 (2003). [PubMed: 14676325]
26. Shangguan D et al. Aptamers evolved from live cells as effective molecular probes for cancer study. Proc. Natl. Acad. Sci. U. S. A. 103, 11838–11843 (2006). [PubMed: 16873550]
27. Ogasawara D, Hasegawa H, Kaneko K, Sode K & Ikebukuro K Screening of DNA aptamer against mouse prion protein by competitive selection. Prion 1, 248–254 (2007). [PubMed: 19164908]
28. Sefah K, Shangguan D, Xiong X, O'Donoghue MB & Tan W Development of DNA aptamers using Cell-SELEX. Nat. Protoc. 5, 1169–1185 (2010). [PubMed: 20539292]
29. Alam KK, Chang JL & Burke DH FASTAptamer: A Bioinformatic Toolkit for High-throughput Sequence Analysis of Combinatorial Selections. Mol. Ther. Nucleic Acids 4, e230 (2015). [PubMed: 25734917]

30. Caroli J, Taccioli C, De La Fuente A, Serafini P & Bicciato S APTANI: a computational tool to select aptamers through sequence-structure motif analysis of HT-SELEX data. Bioinformatics 32, 161–164 (2015). [PubMed: 26395772]
31. Bailey TL et al. MEME SUITE: tools for motif discovery and searching. Nucleic Acids Res. 37, W202–208 (2009). [PubMed: 19458158]
32. Chen L et al. Aptamer-mediated efficient capture and release of T lymphocytes on nanostructured surfaces. Adv. Mater. 23, 4376–4380 (2011). [PubMed: 21882263]
33. Li S, Chen N, Zhang Z & Wang Y Endonuclease-responsive aptamer-functionalized hydrogel coating for sequential catch and release of cancer cells. Biomaterials 34, 460–469 (2013). [PubMed: 23083933]
34. Xu Y et al. Aptamer-based microfluidic device for enrichment, sorting, and detection of multiple cancer cells. Anal. Chem. 81, 7436–7442 (2009). [PubMed: 19715365]
35. Yoon JW et al. Isolation of Foreign Material-Free Endothelial Progenitor Cells Using CD31 Aptamer and Therapeutic Application for Ischemic Injury. PLoS One 10, e0131785 (2015). [PubMed: 26148001]
36. Zhu J, Nguyen T, Pei R, Stojanovic M & Lin Q Specific capture and temperature-mediated release of cells in an aptamer-based microfluidic device. Lab Chip 12, 3504–3513 (2012). [PubMed: 22854859]
37. Labib M et al. Aptamer and Antisense-Mediated Two-Dimensional Isolation of Specific Cancer Cell Subpopulations. J. Am. Chem. Soc. 138, 2476–2479 (2016). [PubMed: 26860321]
38. Sun N et al. Chitosan Nanofibers for Specific Capture and Nondestructive Release of CTCs Assisted by pCBMA Brushes. Small 12, 5090–5097 (2016). [PubMed: 27445096]
39. Wan Y et al. Capture, isolation and release of cancer cells with aptamer-functionalized glass bead array. Lab Chip 12, 4693–4701 (2012). [PubMed: 22983436]
40. Zhang Z, Chen N, Li S, Battig MR & Wang Y Programmable hydrogels for controlled cell catch and release using hybridized aptamers and complementary sequences. J. Am. Chem. Soc. 134, 15716–15719 (2012). [PubMed: 22970862]
41. Nozari A & Berezovski MV Aptamers for CD Antigens: From Cell Profiling to Activity Modulation. Mol. Ther. Nucleic Acids 6, 29–44 (2017). [PubMed: 28325295]
42. Wang C-W et al. A new nucleic acid–based agent inhibits cytotoxic T lymphocyte–mediated immune disorders. J. Allergy Clin. Immunol. 132, 713–722. e711 (2013). [PubMed: 23791505]
43. Seelig G, Soloveichik D, Zhang DY & Winfree E Enzyme-free nucleic acid logic circuits. Science 314, 1585–1588 (2006). [PubMed: 17158324]
44. Yurke B & Mills AP Using DNA to power nanostructures. Genet Program Evol M 4, 111–122 (2003).
45. Yurke B, Turberfield AJ, Mills AP Jr., Simmel FC & Neumann JL A DNA-fuelled molecular machine made of DNA. Nature 406, 605–608 (2000). [PubMed: 10949296]
46. Zhang DY & Seelig G Dynamic DNA nanotechnology using strand-displacement reactions. Nat. Chem. 3, 103–113 (2011). [PubMed: 21258382]
47. Zhang DY & Winfree E Control of DNA strand displacement kinetics using toehold exchange. J. Am. Chem. Soc. 131, 17303–17314 (2009). [PubMed: 19894722]
48. Ruella M et al. Induction of resistance to chimeric antigen receptor T cell therapy by transduction of a single leukemic B cell. Nat. Med. 24, 1499–1503 (2018). [PubMed: 30275568]
49. Heczey A et al. Invariant NKT cells with chimeric antigen receptor provide a novel platform for safe and effective cancer immunotherapy. Blood 124, 2824–2833 (2014). [PubMed: 25049283]
50. Eyquem J et al. Targeting a CAR to the TRAC locus with CRISPR/Cas9 enhances tumour rejection. Nature 543, 113–117 (2017). [PubMed: 28225754]
51. Zhao Z et al. Structural Design of Engineered Costimulation Determines Tumor Rejection Kinetics and Persistence of CAR T Cells. Cancer Cell 28, 415–428 (2015). [PubMed: 26461090]
52. Brentjens RJ et al. Eradication of systemic B-cell tumors by genetically targeted human T lymphocytes co-stimulated by CD80 and interleukin-15. Nat. Med. 9, 279–286 (2003). [PubMed: 12579196]

53. Dahotre SN, Chang YM, Wieland A, Stammen SR & Kwong GA Individually addressable and dynamic DNA gates for multiplexed cell sorting. Proc. Natl. Acad. Sci. U. S. A. 115, 4357–4362 (2018). [PubMed: 29632190]

54. Probst CE, Zrazhevskiy P & Gao X Rapid multitarget immunomagnetic separation through programmable DNA linker displacement. J. Am. Chem. Soc. 133, 17126–17129 (2011). [PubMed: 21988124]

55. Gawande BN et al. Selection of DNA aptamers with two modified bases. Proc. Natl. Acad. Sci. U. S. A. 114, 2898–2903 (2017). [PubMed: 28265062]

56. Ni S et al. Chemical Modifications of Nucleic Acid Aptamers for Therapeutic Purposes. Int. J. Mol. Sci. 18, 1683 (2017).

57. Pelloquin F, Lamelin J & Lenoir G Human blymphocytes immortalization by epstein-barr virus in the presence of cyclosporin a. In Vitro Cell. Dev. Biol. 22, 689–694 (1986).

58. Zadeh JN et al. NUPACK: Analysis and design of nucleic acid systems. J. Comput. Chem. 32, 170–173 (2011). [PubMed: 20645303]

59. Tsai HH et al. Regional astrocyte allocation regulates CNS synaptogenesis and repair. Science 337, 358–362 (2012). [PubMed: 22745251]

60. Madugula V & Lu L A ternary complex comprising transportin1, Rab8 and the ciliary targeting signal directs proteins to ciliary membranes. J. Cell Sci. 129, 3922–3934 (2016). [PubMed: 27633000]

61. Wang J et al. Optimizing adoptive polyclonal T cell immunotherapy of lymphomas, using a chimeric T cell receptor possessing CD28 and CD137 costimulatory domains. Hum. Gene Ther. 18, 712–725 (2007). [PubMed: 17685852]

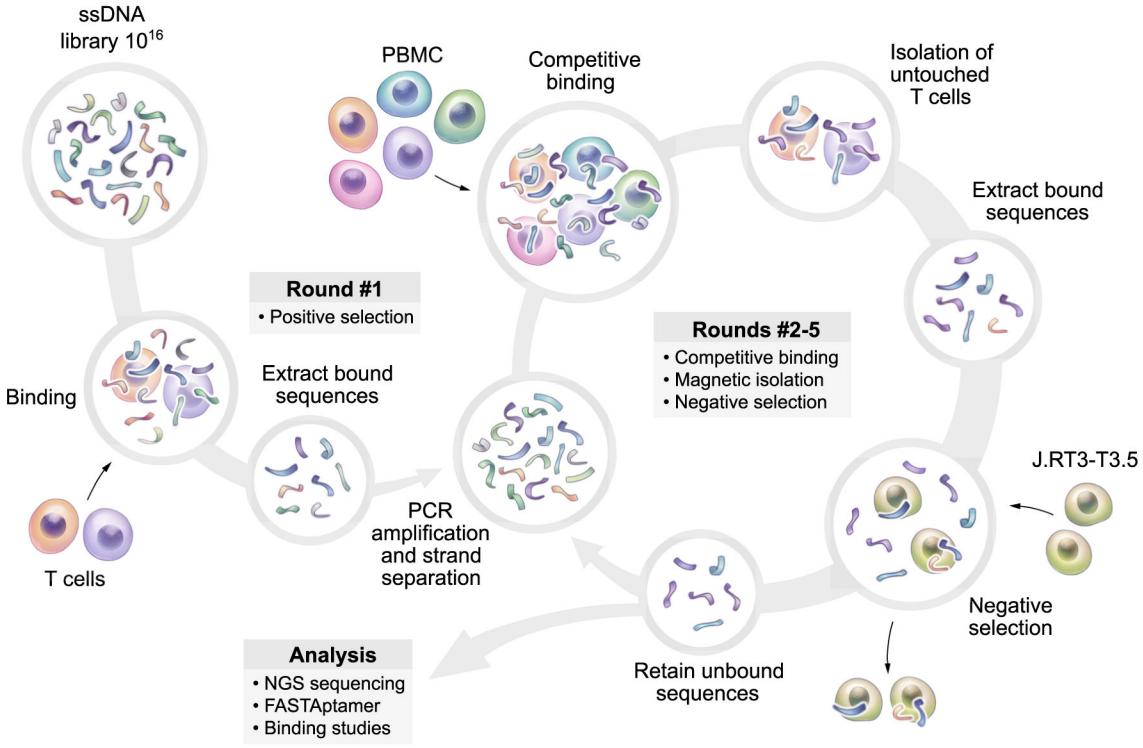

Fig. 1 | Schematic representation of competitive cell-SELEX with magnetic depletion from PBMCs.

A DNA aptamer library underwent one round of positive selection against mixed T cells followed by four rounds of consecutive competitive selection and negative selection against PBMCs and $CD4^{lo}CD8^{-}$ J.RT3-T3.5 cells, respectively, under increasingly stringent conditions. After competitive selection, untouched T cells and bound aptamers were isolated from PMBCs by depleting non-target cell using a Pan T Cell Isolation Kit.

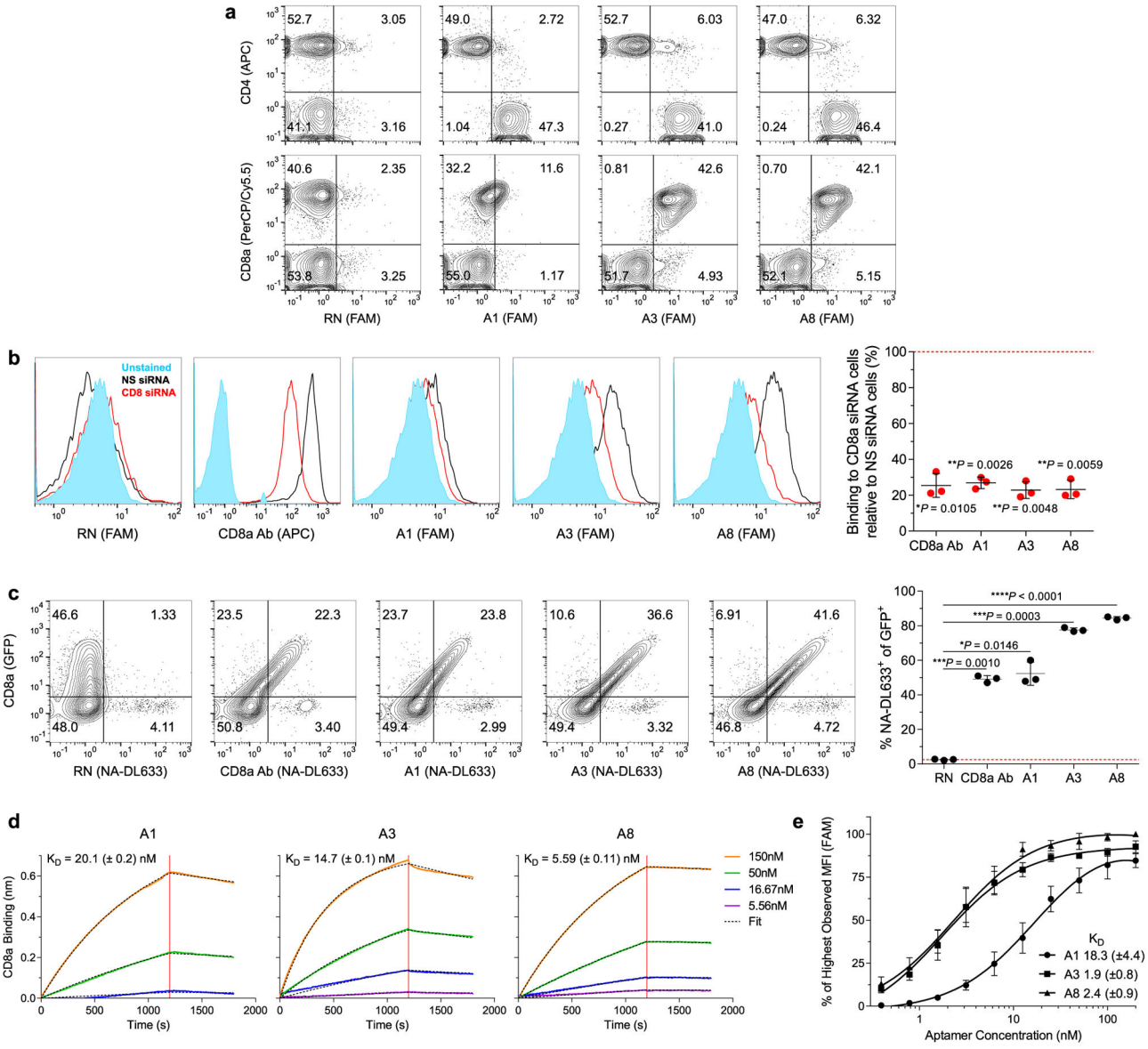

Fig. 2 | Aptamers 1, 3, and 8 bind to CD8a glycoprotein.

a, Flow cytometry plots of 50nM random (RN), A1, A3, and A8 aptamer binding to $CD4^+$ and $CD8^+$ T cells in a mixed T cell population. Plots are representative of 1 independent experiment. **b**, Flow cytometry analysis of CD8a antibody (CD8a Ab) and 10nM RN, A1, A3, and A8 aptamer binding to $CD8^+$ T cells 24 hours after nucleofection with non-specific (NS) siRNA or CD8 siRNA duplexes. Histograms are representative of 3 independent experiments with technical triplicates. Chart indicates binding to CD8 siRNA-treated cells relative to NS siRNA treated controls. Data are mean ± s.d., $n = 3$ independent experiments, $^*P < 0.05$ and $^{**}P < 0.01$ (one-way ANOVA with Bonferroni correction). **c**, Flow cytometry analysis of CD8a Ab and 10nM RN, A1, A3, and A8 aptamer binding to $CD8^-$ Jurkat cells 24 hours after nucleofection with a CD8a-hnRNP-M-EGFP plasmid. Plots are representative of 3 biological replicates with technical triplicates. Chart indicates percentage of GFP^+ Jurkats that were also positive for antibody or aptamer binding. Data are mean ± s.d., $n = 3$

biologically independent samples, $*P < 0.05$, $***P < 0.001$, and $****P < 0.0001$ (paired one-way ANOVA with Dunnett's test). **d**, BLI measured association and dissociation kinetics of serially diluted CD8a protein binding to immobilized A1, A3, and A8 aptamers. The association phase is illustrated from 0 to 1200 seconds, whereas dissociation is shown from 1200-1800 seconds. K_D's were calculated by performing a global fit of the kinetic data at the different concentrations of CD8a protein to a 1:1 binding model. K_D's are mean ± s.d., $n = 3$ individual concentrations for A1 and 4 individual concentrations for A3 and A8. **e**, Flow cytometry binding curves of A1, A3, and A8 aptamers to $CD8^+$ T cells, normalized to 200nM of A8 binding. Curves represent a non-linear regression assuming one site total binding of 3 independent experiments with technical triplicates. K_D's were calculated by averaging the individual regressions values of the independent experiments. Curves and K_D's are mean ± s.d., $n = 3$ independent experiments.

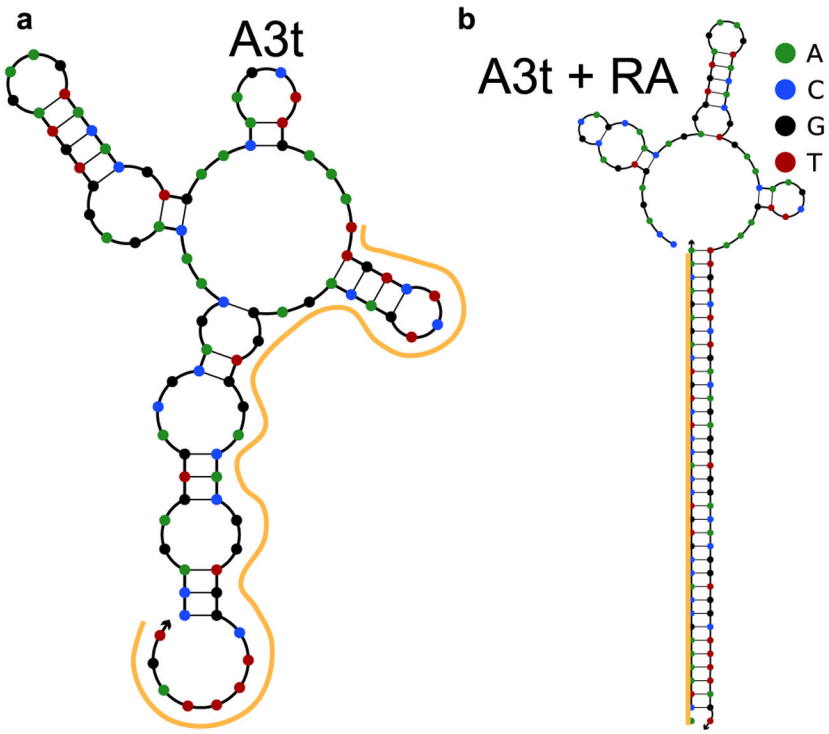

Fig. 3 |. Complementary reversal agent designed to occlude binding of A3 aptamer with modified toehold.

a, Predicted minimum free energy (MFE) secondary structure of a modified A3 aptamer with a 3' 8-bp toehold (A3t) using NUPACK software (*temp* = 4C; Na^{+} = 137mM; Mg^{++} = 5.5mM). The orange line represents the 36-bp region that a complementary reversal agent (RA) was designed to anneal. **b,** Predicted MFE secondary structure of the A3t aptamer after strand displacement with the RA (*temp* = 20C; Na^{+} = 137mM; Mg^{++} = 5.5mM).

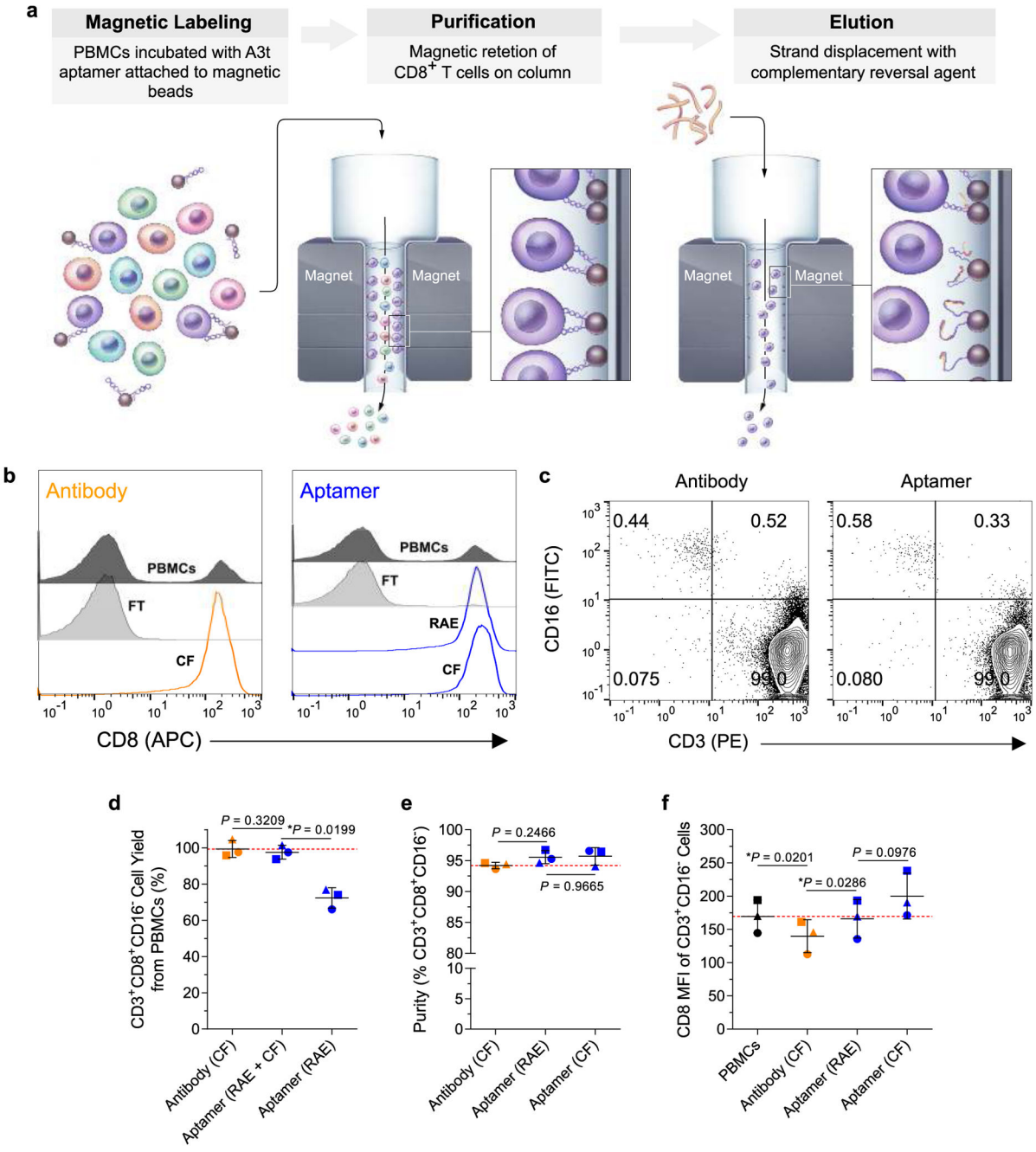

Fig. 4 |. Isolation of label-free CD8$^+$ T cells from PBMCs using a reversible, aptamer-based selection strategy.

a, Schematic representation of traceless selection of CD8$^+$ T cells using the A3t aptamer. Biotinylated aptamer (5nM) pre-loaded onto Miltenyi Anti-Biotin Microbeads was incubated with PBMCs to magnetically label CD8$^+$ T cells. The cell suspension was applied onto an LS Column under a magnetic field, in which unlabeled cells were removed in the flow through (FT) fraction. Microbead labeled CD8$^+$ T cells that remain on the column are incubated with 100X excess of complementary RA, and released CD8$^+$ T cells are washed off the column in the RA elution (RAE) fraction. Remaining cells on the column are

removed using a plunger column flush (CF) in the absence of the magnetic field. **b**, Flow cytometry histograms of CD8 expression in the different fractions of standard, antibody-based Miltenyi CD8 Microbead isolation and traceless aptamer-based isolation. Histograms are representative of 3 independent experiments with technical triplicates. **c**, Flow cytometry plots of CD3 and CD16 expression in $CD8^+$ antibody-isolated CF and aptamer-isolated RAE cell fractions to distinguish between $CD3^+$ $CD16^-$ T cells and $CD3^-CD16^+$ monocytes and NK cells. Plots are representative of 3 independent experiments with technical triplicates. **d-f**, Flow cytometry analysis of yield, purity, and CD8 MFI of $CD3^+CD8^+CD16^-$ T cells in different fractions of antibody- and aptamer-based isolations. Symbols represent different donors from separate isolation experiments, and all data was collected in technical triplicates. Data are mean ± s.d., $n = 3$, $P > 0.05$ and $^*P < 0.05$ (**d-f**, paired one-way ANOVA with Tukey's test).

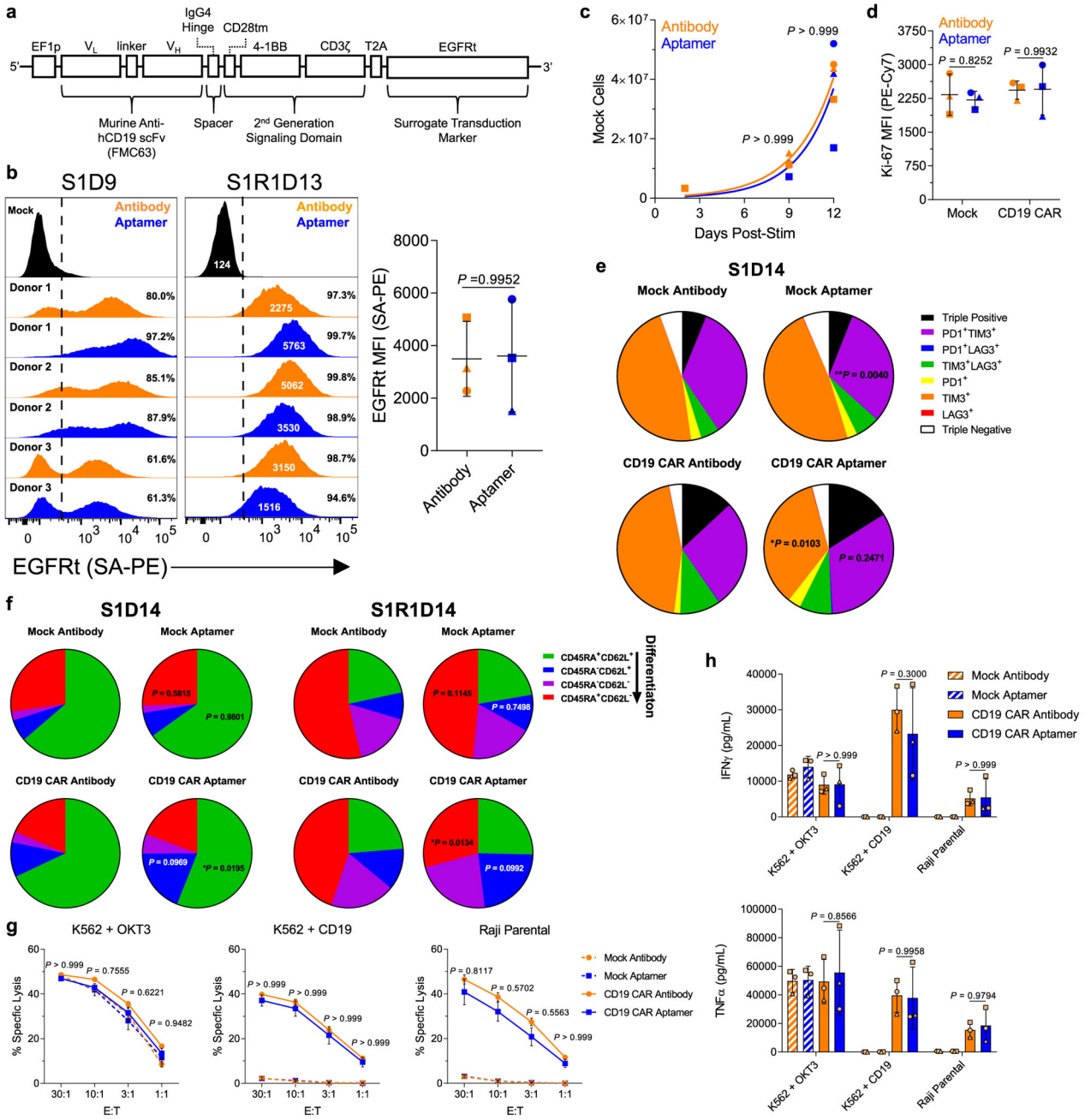

Fig. 5 | Characterization of CD19 CAR T cells generated from antibody- and aptamer-isolated cells.

a, 2nd generation CD19 CAR T cell construct with EGFRt reporter used to retrovirally transduce isolated T cells. **b**, Flow cytometry analysis of EGFRt expression in antibody- and aptamer-isolated T cells 9-days post initial bead stimulation (S1D9) and 13-days post rapid expansion protocol (REP, S1R1D13) with irradiated $CD19^+$ TM-LCL cells. Timeline of cell expansion is shown in Supplementary Fig. 12. Chart indicates EGFRt reporter MFI at S1R1D13, with symbols as in Fig. 4d-f. Flow histograms are representative of 1 independent experiment. Data are mean ± s.d., $n = 3$, $P > 0.05$ (two-sided paired t-test). **c,** Growth of non-

transduced mock T cells post bead stimulation. Symbols as in Fig. 4d-f, $n = 3$, $P > 0.05$ (paired two-way ANOVA with Bonferroni correction). Curves represent a least-squares fit to the exponential growth equation. **d**, Flow cytometry analysis of Ki-67 expression in mock and CD19 CAR T cells on S1D14 immediately before REP. Symbols as in Fig. 4d-f. Data are mean ± s.d., $n = 3$, $P > 0.05$ (paired two-way ANOVA with Sidak correction). **e**, Flow cytometry analysis PD1/TIM3/LAG3 expression in mock and CD19 CAR T cells on S1D14 immediately before REP. Individual donor values can be found in Supplemental Fig. 14. Pie charts show the mean phenotype of the cells, $n = 3$ biologically independent samples, $P > 0.05$, $*P < 0.05$, and $**P < 0.01$ (paired two-way ANOVA with Bonferroni correction). **f,** Flow cytometry analysis of CD62L/CD45RA expression in mock and CD19 CAR T cells on S1D14 immediately before REP and on S1R1D14 immediately before functional assays. Individual donor values can be found in Supplemental Fig. 15. Pie charts show the mean phenotype of the cells, $n = 3$ biologically independent samples, $P > 0.05$ and $*P < 0.05$ (paired two-way ANOVA with Bonferroni correction). **g**,**h**, *In vitro* anti-tumor cytotoxicity and cytokine release of mock and CD19 CAR T cells. For **h**, symbols as in Fig. 4d-f. Data are mean ± s.d., $n = 3$ biologically independent samples, $P > 0.05$ (**g,** paired two-way ANOVA with Bonferroni correction; **h**, paired two-way ANOVA with Sidak correction).

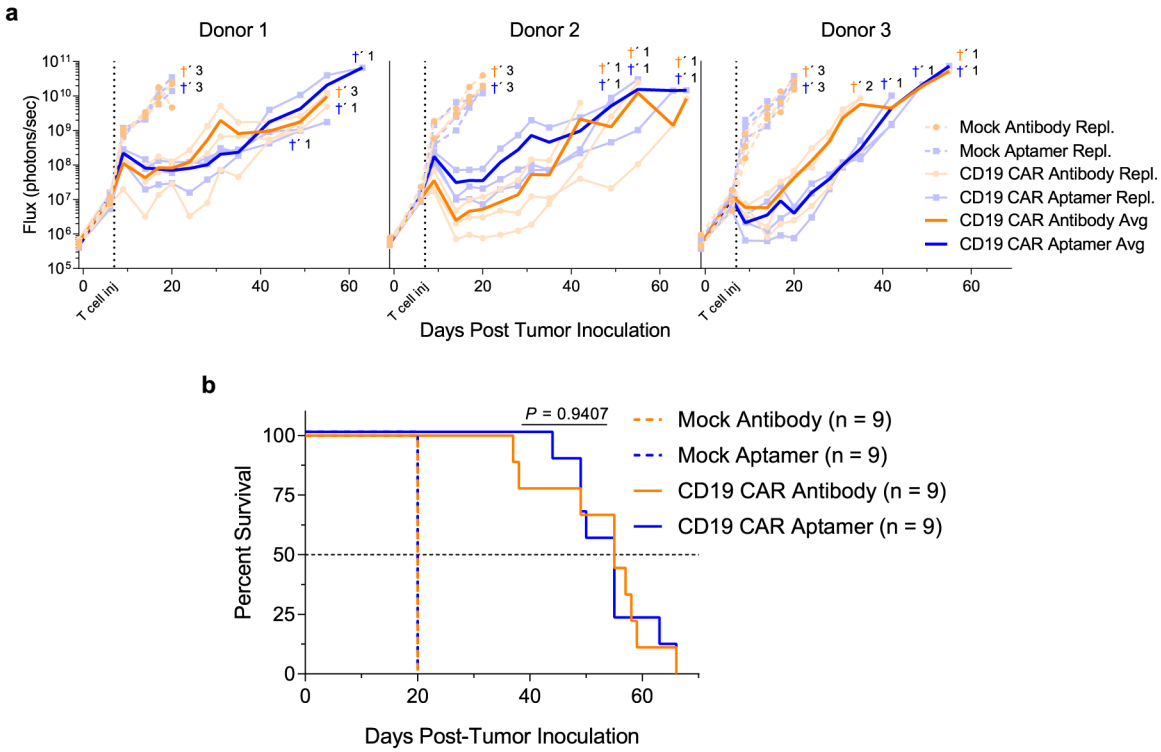

Fig. 6 | Tumor stress test with antibody- and aptamer-isolated CD8$^+$ CD19 CAR T cells.
NSG mice were inoculated intravenously (i.v.) with 5×10^5 CD19$^+$ Raji cells and treated 7 days later with 10^7 CD8$^+$ mock or CD19 CAR T cells from antibody- or aptamer-isolated donor cells. **a**, Flux of the systemic tumors. The "†" symbol represents euthanasia of individual mice. The faint curves are the tumor flux values for the individual mice (3 mice per donor per group), whereas the bold curves are the mean flux values for the respective CD19 CAR T cell treatment groups over time. **b**, Kaplan-Meier survival curves. Median survival time (days) of the CD19 CAR T cell treatment groups were as follows; antibody: 55; aptamer: 55. $n = 9$ (3 mice per donor), $P > 0.05$ (two-sided log-rank test).